Nanoscale Advances

ROYAL SOCIETY OF CHEMISTRY

PAPER

View Article Online
View Journal | View Issue

Cite this: *Nanoscale Adv.*, 2026, **8**, 937

Bimetallic $Ti_3C_2T_x$ with three synergistic catalytic pathways and enhanced dual enzyme activities for a visual sensing platform

Zhiren Zhou, †[ae] Lina Zou,†[b] Ping Zhang,[a] Jing Dong,[a] Jian Zhou,[c] Hao Jiang,[c] Huanyu Ren,[a] Zheng Li,[a] Huiru Niu,[a] Hao Liao,[a] Xiaojing Zhang,[a] Shanshan An,[a] Fei Ren,[a] Xiuhong Ge,[a] Lang Cheng,[a] Feiyan Yang,[a] Hongzhi Pan,[cd] Shengzhong Rong*[a] and Hongkun Ma*[a]

Nano-enzymes are increasingly used in forensic identification, biochemical testing, food regulation, environmental pollution monitoring and other fields. However, the construction of enzyme cascade catalytic systems based on nano-enzymes with multiple enzyme activities presents both opportunities and challenges. Ti_3AlC_2 is a common MXene with a graphene-like structure, which has the features of a large specific surface area, good electrical conductivity, excellent catalytic properties, and easy functionalization. Moreover, after being functionalized, Ti_3AlC_2 can exhibit excellent peroxidase-like activity. Therefore, in this work, a bimetallic Fe–Ni@$Ti_3C_2T_x$ nano-enzyme with both peroxidase-like and oxidase-like activities was synthesized, and three synergistic catalytic mechanisms of Fe–Ni@$Ti_3C_2T_x$ were verified. A colorimetric sensor was constructed based on Fe–Ni@$Ti_3C_2T_x$ for the detection of H_2O_2 to test its feasibility for practical applications. The prepared colorimetric sensor had a wide linear range (50–6000 μM) and a low detection limit (14.606 μM). In addition, the selectivity, stability and reproducibility of the prepared colorimetric sensor were acceptable. This study laid a foundation for the simple preparation and practical application of a bimetallic nano-enzyme with various enzyme activities.

Received 3rd October 2025
Accepted 1st December 2025

DOI: 10.1039/d5na00939a

rsc.li/nanoscale-advances

1 Introduction

Nano-enzymes are chemically synthesized nanomaterials with natural biological enzyme activity. Compared with natural enzymes, nano-enzymes are characterized by the properties of nanomaterials, including easy synthesis, easy storage, high stability and low cost, in addition to enzyme-like activity.[1] Distinct nanomaterials, including carbon-based nanomaterials, transition metal oxides, and metals, have successfully mimicked various natural enzymes, such as peroxidase, oxidase, catalase, and superoxide dismutase, biologically.[2–4] Therefore, nano-enzymes are widely used in biochemical detection,[5] anti-tumor therapy,[6] environmental engineering,[7] and food regulation.[8] Nano-enzymes with dual activities are more conducive to practical applications. Among them, nano-enzymes with both peroxidase-like and oxidase-like activities belong to a more important category, which can skillfully constitute a cascade reaction system between the two enzyme activities, realize the self-sufficiency of the intermediate product H_2O_2 and constitute a closed-loop reaction, greatly improving the reaction efficiency.[9]

Two-dimensional layered nanomaterials (MXenes, black phosphorus, and graphitized carbon nitrides) show enormous potential application in the domain of nano-enzymes due to their large specific surface area, excellent physicochemical properties, and unique nanosheet structures.[10–12] MXene is a two-dimensional material with a graphene-like structure, consisting of transition metal carbides, nitrides or carbon-nitrides.[13] The chemical formula is $M_{n+1}X_nT_x$, where M represents a transition metal element, X represents carbon, nitrogen and their mixture, and T_x represents a surface functional group, such as –F, –Cl, =O, or –OH.[14] Due to the unique physico-chemical properties, such as a large specific surface area, good electrical conductivity, excellent catalytic properties, and ease of functionalization, MXenes have been widely used in many fields, including biomedicine,[15] energy storage,[16] catalysis,[17] and sensors.[18] The special hexagonal crystal system and lamellar structure endow Ti_3AlC_2 with properties of high electric conductivity, high thermal conductivity, ease of processing, corrosion resistance, and good thermal shock resistance.[19] However, the defects of easy oxidation, easy stacking between

[a]*Public Health School, Mudanjiang Medical University, Mudanjiang, China. E-mail: sz_rong@yeah.net; mahongkunmdjmu@163.com*
[b]*Nursing School Mudanjiang Medical University, Mudanjiang, China*
[c]*Affiliated Hongqi Hospital, Mudanjiang Medical University, Mudanjiang, China*
[d]*Collaborative Research Center Shanghai University of Medicine and Health Sciences, Shanghai, China*
[e]*Centers for Disease Control and Prevention, BaZhong, China*
† These authors contributed equally to this work.

layers and poor biocompatibility of Ti_3AlC_2 limit its application. Combining Ti_3AlC_2 with nanoparticles, metal particles, and non-metallic ions can improve these drawbacks.[20] The functionalized Ti_3AlC_2 exhibits peroxidase-like activity, which can catalyze the production of –OH from H_2O_2 and then oxidize TMB with a color change (colorless to blue).[21] Therefore, colorimetric sensors based on Ti_3AlC_2 are favored by researchers. Geng *et al.* demonstrated the synergistically enhanced catalytic activity of Ti_3C_2/Pt composites for the specific detection of glutathione and glucose based on the inhibition effect and cascade reactions, respectively.[4] Li *et al.*, using an *in situ* co-precipitation method, synthesized a MXene@NiFe-LDH nanohybrid material with strong peroxidase-like activity and successfully realized the detection of glutathione.[22] Thus, functionalized MXene materials exhibit better performance.

Single-atom nano-enzymes (SA-zymes) are characterized by unique electronic structure, clear geometry, and high atom utilization efficiency.[23] Xi *et al.* loaded Fe atoms on $Ti_3C_2T_x$ to form a single-atom nano-enzyme Fe–SA/$Ti_3C_2T_x$ with excellent peroxidase-like activity, which achieved one-time recognition of five antioxidants.[24] Specifically, on $Ti_3C_2T_x$, the element Fe existed in atomic form, with one Fe atom coordinated by three oxygen atoms. The strong interaction between Fe atoms and $Ti_3C_2T_x$ through Fe–O–Ti ligands promoted the electron transfer from Fe–SA/$Ti_3C_2T_x$ to H_2O_2, which in turn enhanced the peroxidase-like activity. However, SA-zymes suffer from the deficiency of low loading, which can be solved by bimetallic nano-enzymes and enhance the peroxidase-like activity by the synergistic effect.[25] Ni is a transition metal with a small atomic radius, low electronegativity, and more valence states, in which the d-electron layer is prone to losing or capturing electrons.[26] Ni, owing to the advantages of its strong redox properties, stable chemical properties, and low cost, has been used to design a variety of nano-enzymes.[27] Therefore, the Fe–Ni bimetallic nano-enzyme may have better performance.

Based on the above discussion, in this work, Fe and Ni were loaded on $Ti_3C_2T_x$ in a simple method for the first time. Fe–Ni@$Ti_3C_2T_x$ exhibits strong peroxidase-like and oxidase-like activity, consuming H_2O_2 while generating H_2O_2, greatly amplifying the signal (Fig. 1).

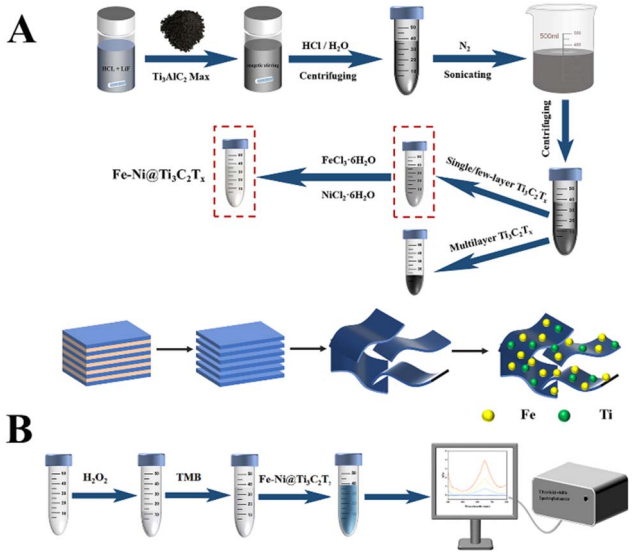

Fig. 1 Synthesis of Fe–Ni@$Ti_3C_2T_x$ (A) and colorimetric detection of H_2O_2 (B).

2 Experimental section

2.1 Materials

Ti_3AlC_2 was bought from Suzhou Beike Nanotechnology Co., Ltd (Jiangsu, China). Lithium fluoride (LiF), iron chloride hexahydrate ($FeCl_3 \cdot 6H_2O$), and nickel chloride hexahydrate ($NiCl_2 \cdot 6H_2O$) were bought from Aladdin Reagent Co., Ltd (Shanghai, China). Hydrochloric acid (HCl), TMB, and H_2O_2 were purchased from Beijing Solarbio Science & Technology Co., Ltd (Beijing, China).

2.2 Instrumentation

Transmission electron microscopy (TEM) was performed on Tecnai G2 F20 (FEI, USA). The environment control scanning probe microscope (AFM) was from Nanonavi E-Sweep (SII, Japan). Transmission electron microscopy mapping (SEM-Mapping) was performed using QUANTA FEG 250 (FEI, USA). Energy dispersive spectroscopy (EDS) was performed using a UH5300 spectrophotometer (HITACHI, Japan). X-ray diffraction (XRD) was carried out using D8 ADVANCE X (Bruker, Germany). X-ray photoelectron spectroscopy (XPS) was performed by Axis Ultra DLD (Kratos, England). The absorption spectra were recorded on a TU-1901 ultraviolet (UV) spectrophotometer (Purkinje, China). Ultra-pure water was obtained by Milli-Q purification system (Merck Millipore, Germany), which was used throughout the entire experiment.

2.3 Synthesis of $Ti_3C_2T_x$

Ti_3AlC_2 was synthesized according to a reported method with slight modifications.[24] LiF (3.2 g) was added to HCl (12 M 40 mL) and heated to 45 °C with stirring for 10 min. Ti_3AlC_2 (2 g) was added to the above mixed solution and stirred magnetically at 45 °C for 48 h. The solution was then poured into a centrifuge tube and centrifuged for 5 min. The above solution was rinsed three times with dilute HCl (2 M), followed by several rinses with ultra-pure water until the pH of the upper layer was close to 6 (centrifugation at 3500 rpm for 5 min was performed to ensure a thorough separation of the upper liquid from the precipitate). Next, the mixture was poured into a gas collection flask and sonicated under nitrogen and ice bath conditions for 1 h. Finally, the mixture was poured into a centrifuge tube and centrifuged for 45 min. The upper layer of the black liquid comprised single/few-layer $Ti_3C_2T_x$ nanosheets, which were sealed and stored in the refrigerator at 4 °C for use.

2.4 Synthesis of Fe–Ni@$Ti_3C_2T_x$

The fabrication of Fe–Ni@$Ti_3C_2T_x$ was carried out with slight modifications on the basis of an existing study.[24] $FeCl_3 \cdot 6H_2O$ (6

mg) and $NiCl_2 \cdot 6H_2O$ (9 mg) were added to $Ti_3C_2T_x$ (10 mL), stirred for 10 min and sonicated for 30 min to obtain Fe–Ni@$Ti_3C_2T_x$ peroxidase, and the synthetic material was then preserved in a lightproof refrigerator (4 °C) (Fig. 1A).

2.5 Preparation of the sensor

The preparation was completed by first adding H_2O_2 (0.5 mL), then TMB (3.5 mL) and finally Fe–Ni@$Ti_3C_2T_x$ (1 mL) to an empty test tube. Measurements were carried out under optimum experimental conditions (50 °C, 13 min, pH = 3) using a UV spectrophotometer, as shown in Fig. 1B.

3 Results and discussion

3.1 Optimization and characterization of synthesized materials

3.1.1 The quality optimization of $FeCl_3 \cdot 6H_2O$ and $NiCl_2 \cdot 6H_2O$. The modulation of the Fe/Ni ratio tailors the electronic configuration of bimetallic active sites, including charge-density redistribution and interfacial bonding modes between Fe and Ni, thereby reinforcing the synergistic catalytic efficacy.[28] The balanced Fe/Ni proportion can also optimize the enzymatic-like reaction kinetics and ameliorate the structural stability of the composite, which enhances its anti-interference capability.[29] Keeping the experimental conditions unchanged (0.5 mL 100 μM H_2O_2, 3.5 mL TMB, 1 mL Fe–Ni@$Ti_3C_2T_x$, 50 °C, 13 min, pH = 3), the Fe and Ni contents in Fe–Ni@$Ti_3C_2T_x$ were optimized. $FeCl_3 \cdot 6H_2O$ (1, 3, 6, 9, 12 mg) and 9 mg $NiCl_2 \cdot 6H_2O$ were added to 10 mL of $Ti_3C_2T_x$, respectively, with stirring for 10 min and ultrasonication for 30 min. It can be noted from Fig. S1A that the strongest absorption peak and the highest absorbance were obtained when $FeCl_3 \cdot 6H_2O$ was 6 mg per 10 mL of $Ti_3C_2T_x$. Under the same experimental conditions, $NiCl_2 \cdot 6H_2O$ (1, 3, 6, 9, 12 mg) and 6 mg $FeCl_3 \cdot 6H_2O$ were added to five 10 mL $Ti_3C_2T_x$, stirred for 10 min, and ultrasonicated for 30 min. The optimum absorption peak and the highest absorbance were obtained with 9 mg of $NiCl_2 \cdot 6H_2O$. In brief, with 6 mg $FeCl_3 \cdot 6H_2O$ and 9 mg $NiCl_2 \cdot 6H_2O$ per 10 mL of $Ti_3C_2T_x$, the strongest absorption peak can be obtained and Fe–Ni@$Ti_3C_2T_x$ exhibits the highest peroxidase activity (Fig. S1B).

3.1.2 Characterization of $Ti_3C_2T_x$ and Fe–Ni@$Ti_3C_2T_x$. The morphology of $Ti_3C_2T_x$ was characterized by TEM and AFM. As shown in Fig. 2A(a and b), the prepared $Ti_3C_2T_x$ was composed of layered nanosheets. AFM images revealed that the surface of $Ti_3C_2T_x$ exhibited nanoscale roughness, with a maximum peak-to-valley height difference of approximately 7.1 nm and an average surface fluctuation of about 1.9 nm (Fig. 2A(c)). The surface roughness of $Ti_3C_2T_x$ contributes to enhanced metal adsorption capacity, thereby improving its catalytic performance. XRD and XPS data were in agreement with those reported in the study, which further confirmed the successful synthesis of single/few-layer $Ti_3C_2T_x$ nanosheets as shown in

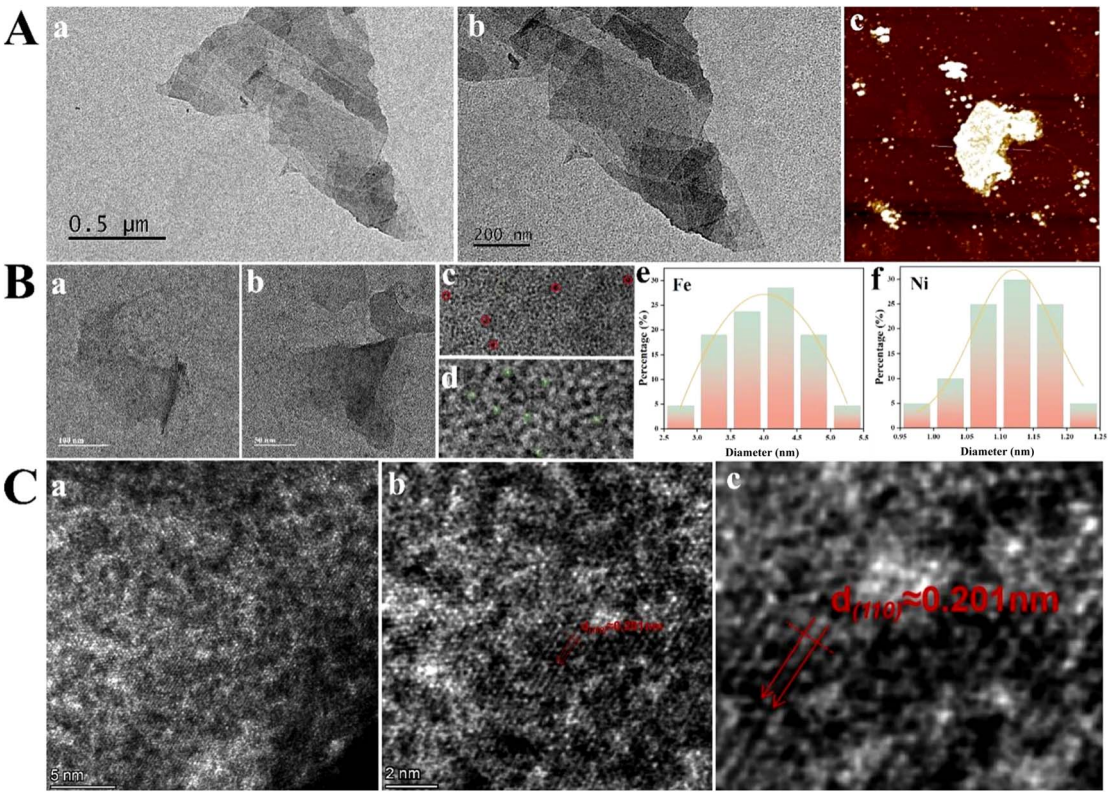

Fig. 2 (A) Characterization of $Ti_3C_2T_x$. TEM (a and b) and AFM images (c). (B) Characterization of Fe–Ni@$Ti_3C_2T_x$. TEM images of Fe–Ni@$Ti_3C_2T_x$ (a and b), Fe nanoparticles (c) and Ni nanoparticles (d) and size distribution of Fe nanoparticles (e) and Ni nanoparticles (f). (C) AC HAADF-STEM image of Fe–Ni@$Ti_3C_2T_x$. With a scale bar of 5 nm (a) and 2 nm (b), and (c) magnified view of the cropped region from (b).

Fig. S3A and C.[24] As illustrated in Fig. 2B(a and b), the TEM of Fe–Ni@$Ti_3C_2T_x$ showed that Fe–Ni@$Ti_3C_2T_x$ retained a good nanosheet structure, and Fe–Ni nanoparticles were observed to be uniformly dispersed on $Ti_3C_2T_x$ nanosheets. Fig. 2B(c) shows Fe nanoparticles on the $Ti_3C_2T_x$ surface, while Fig. 2B(d) shows Ni nanoparticles on the $Ti_3C_2T_x$ surface. Fig. 2B(e and f) confirms the uniform distribution of Fe and Ni nanoparticles across the $Ti_3C_2T_x$ surface, with average particle sizes of 4.000 nm for Fe and 1.123 nm for Ni. As shown in Fig. 2C(a–c), a large number of spots in the aberration-corrected HAADF-STEM (AC-HAADF-STEM) indicated the presence of Fe and Ni nanoparticles on Fe–Ni@$Ti_3C_2T_x$. The lattice fringes observed in the images correspond to the (110) crystal plane of Fe. The EDS mapping demonstrated that the elements of C, Ti, O, Fe, and Ni were homogeneously distributed on Fe–Ni@$Ti_3C_2T_x$ (Fig. S2). In addition, the elemental composition of the Fe–Ni@$Ti_3C_2T_x$ surface and its chemical state were analyzed by XRD and XPS, as shown in Fig. S3B and D. XRD showed diffraction peaks related to Fe^{2+} and Ni^{2+} compounds. XPS showed a distinct peak at 710.4 eV, corresponding to Fe 2p, and at 855.6 eV, corresponding to Ni 2p, which further proved the presence of Fe^{2+} and Ni^{2+} compounds in Ni@$Ti_3C_2T_x$.[30,31]

3.2 The performance advantages of Fe–Ni@$Ti_3C_2T_x$

3.2.1 Verification of dual enzyme activities of Fe–Ni@$Ti_3C_2T_x$. Based on the following principles: (1) peroxidase-like activity can change TMB from colorless to blue oxTMB in the TMB/H_2O_2 system; (2) oxidase-like activity can directly change TMB from colorless to blue oxTMB; (3) a strong absorption peak at 650 nm can be observed when Fe–Ni@$Ti_3C_2T_x$ has peroxidase-like or oxidase-like activities. The following sets of experiments were designed to validate the dual enzyme activities of Fe–Ni@$Ti_3C_2T_x$: (1) H_2O_2 + Fe–Ni@$Ti_3C_2T_x$; (2) TMB + H_2O_2; (3) TMB + Fe–Ni@$Ti_3C_2T_x$; and (4) TMB + H_2O_2 + Fe–Ni@$Ti_3C_2T_x$ under optimal experimental conditions (0.5 mL 100 μM H_2O_2, 3.5 mL TMB, 1 mL Fe–Ni@$Ti_3C_2T_x$/ultra-pure water, 50 °C, 13 min, pH = 3). The UV-vis adsorption spectra of different reaction systems are shown in Fig. S4. After the addition of Fe–Ni@$Ti_3C_2T_x$ to the TMB/H_2O_2 system, colorless TMB turned into blue oxTMB, and the absorption peak at 650 nm in the UV-vis spectrum appeared much higher than that of other experimental groups, indicating that Fe–Ni@$Ti_3C_2T_x$ has strong peroxidase-like activity. The TMB + Fe–Ni@$Ti_3C_2T_x$ system also showed the absorption peak at 650 nm, but with a lower intensity than that of the TMB + H_2O_2 + Fe–Ni@$Ti_3C_2T_x$ system, suggesting that Fe–Ni@$Ti_3C_2T_x$ had oxidase-like activity, which can catalyze the oxidation of TMB by O_2. Meanwhile, a slight color change and absorption peak were observed in the TMB + H_2O_2 system, indicating the oxidizing property of H_2O_2. The above results confirmed that Fe–Ni@$Ti_3C_2T_x$ possessed strong peroxidase-like and oxidase-like catalytic activity.

3.2.2 The enzyme activity of Fe–Ni@$Ti_3C_2T_x$ is superior to that of $Ti_3C_2T_x$, Fe@$Ti_3C_2T_x$ and Ni@$Ti_3C_2T_x$. Ni@$Ti_3C_2T_x$ was synthesized by adding 9 mg $NiCl_2 \cdot 6H_2O$ to 10 mL $Ti_3C_2T_x$, stirring for 10 min and sonicating for 30 min. Fe@$Ti_3C_2T_x$ was synthesized by mixing 6 mg $FeCl_3 \cdot 6H_2O$ and 10 mL $Ti_3C_2T_x$, stirring for 10 min and sonicating for 30 min. 1 mL of $Ti_3C_2T_x$, Ni@$Ti_3C_2T_x$, Fe@$Ti_3C_2T_x$, and Fe–Ni@$Ti_3C_2T_x$ were added to three test tubes containing 0.5 mL 100 μM of H_2O_2 and 3.5 mL of TMB, respectively, and under the optimal conditions (50 °C, 13 min, pH = 3), the absorbances were detected and the absorption peaks at 650 nm were compared. As demonstrated in Fig. S5, the H_2O_2 +TMB + $Ti_3C_2T_x$, H_2O_2 +TMB + Ni@$Ti_3C_2T_x$, H_2O_2 +TMB + Fe@$Ti_3C_2T_x$, and H_2O_2 +TMB + Fe–Ni@$Ti_3C_2T_x$ systems all showed an obvious absorption peak at 650 nm in the UV-vis spectrogram, but the absorbance and absorption peak at 650 nm of the H_2O_2 + TMB + Fe–Ni@$Ti_3C_2T_x$ system were much higher than those of the $Ti_3C_2T_x$, Ni@$Ti_3C_2T_x$ and Fe@$Ti_3C_2T_x$ systems, suggesting that the enzyme activity of Fe–Ni@$Ti_3C_2T_x$ was superior than those of $Ti_3C_2T_x$, Ni@$Ti_3C_2T_x$ and Fe@$Ti_3C_2T_x$, with Fe–Ni playing a synergistic catalytic role.

3.2.3 The enzyme activity of Fe–Ni@$Ti_3C_2T_x$ is significantly better than that of HRP. Under the optimal experimental conditions, the absorbance of 9 groups of 0.5 mL H_2O_2 + 3.5 mL TMB + 1 mL Fe–Ni@$Ti_3C_2T_x$ system and 9 groups of 0.5 mL H_2O_2 + 3.5 mL TMB + 1 mL HRP system were measured using a UV-vis spectrophotometer. The absorbance (Fig. S6A) and the absorption peak at 650 nm of 0.5 mL H_2O_2 + 3.5 mL TMB + 1 mL Fe–Ni@$Ti_3C_2T_x$ system (Fig. S6B) were significantly higher than that of the 0.5 mL H_2O_2 + 3.5 mL TMB + 1 mL HRP system. Comparison of enzyme activity between Fe–Ni@$Ti_3C_2T_x$ and HRP was performed using a *t*-test of two independent samples, which resulted in $P < 0.05$, verifying that the enzyme activity of Fe–Ni@$Ti_3C_2T_x$ was much stronger than that of HRP.

3.3 Catalytic mechanism of Fe–Ni@$Ti_3C_2T_x$

The catalytic mechanism of Fe–Ni@$Ti_3C_2T_x$ to the H_2O_2/TMB system is presented in Fig. 3. Fe^{2+} can undergo a Fenton reaction with H_2O_2 to produce –OH. Meanwhile, Fe atoms can interact with $Ti_3C_2T_x$ through the Fe–O–Ti ligand to improve the electron transfer ability and catalytic ability, which accelerated the decomposition of H_2O_2 and produced a large amount of –OH.[6] The addition of Ni not only improved the low loading, but also synergized the catalytic reaction and increased the yield of –OH, which further improved the catalytic activity.[32] Therefore, a large quantity of –OH oxidized TMB to produce H_2O and oxTMB, and the solution changed from colorless to blue. In

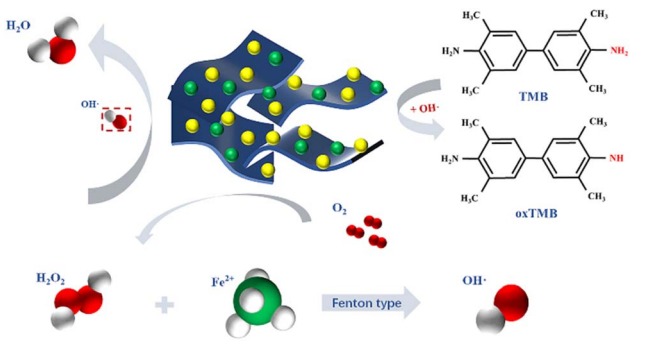

Fig. 3 Catalytic mechanism of Fe–Ni@$Ti_3C_2T_x$.

addition, Fe–Ni@$Ti_3C_2T_x$ is a nano-enzyme with both peroxidase-like and oxidase-like activities, which can combine the ability of oxidase to reduce O_2 to H_2O_2, with the peroxidase to consume H_2O_2 and produce –OH, forming a cascade enzyme-catalyzed system that amplifies the reaction signal.

3.4 Optimization of detection conditions

3.4.1 Optimization of the volume ratio of TMB and Fe–Ni@$Ti_3C_2T_x$. The content of TMB and Fe–Ni@$Ti_3C_2T_x$ had a significant effect on absorbance. In order to control the concentration of H_2O_2, the total volume of the H_2O_2 + TMB + Fe–Ni@$Ti_3C_2T_x$ system was set at 5 mL, and the volume of H_2O_2 was fixed to be 0.5 mL with a concentration of 100 μM. In order to obtain the best volume ratio, the following sets of experiments were designed, including 0.5 mL H_2O_2 + 2 mL TMB + 2.5 mL Fe–Ni@$Ti_3C_2T_x$, 0.5 mL H_2O_2 + 2.5 mL TMB + 2 mL Fe–Ni@$Ti_3C_2T_x$, 0.5 mL H_2O_2 + 3 mL TMB + 1.5 mL Fe–Ni@$Ti_3C_2T_x$, 0.5 mL H_2O_2 + 3.5 mL TMB + 1 mL Fe–Ni@$Ti_3C_2T_x$, and 0.5 mL H_2O_2 + 4 mL TMB + 0.5 mL Fe–Ni@$Ti_3C_2T_x$. As depicted in Fig. S7, under optimal experimental conditions (50 °C, 13 min, pH = 3), the highest absorbance was obtained with the 0.5 mL H_2O_2 + 3.5 mL TMB + 1 mL Fe–Ni@$Ti_3C_2T_x$ system.

3.4.2 Optimization of pH, time, and temperature. The pH, time, and temperature may affect the dual enzyme activities of Fe–Ni@$Ti_3C_2T_x$.[33] The reaction time was defined as the mixing time of Fe–Ni@$Ti_3C_2T_x$ in the H_2O_2/TMB system. In order to confirm the optimal experimental conditions, the absorbance of the system was investigated at different pH (2–6), reaction times (11–15 min) and temperatures (20–60 °C). As illustrated in Fig. S8, pH, reaction time and temperature all had a large effect on the dual enzyme activities of Fe–Ni@$Ti_3C_2T_x$. With the progressively increasing pH, reaction time and temperature, the dual enzyme activities of Fe–Ni@$Ti_3C_2T_x$ initially increased and then decreased. The results demonstrated that the optimal values of pH, reaction time and temperature were 3, 13 min, and 50 °C, respectively.

3.5 Colorimetric detection of H_2O_2

A colorimetric sensor was constructed based on Fe–Ni@$Ti_3C_2T_x$ for the detection of H_2O_2 to test the feasibility of Fe–Ni@$Ti_3C_2T_x$ in practical applications. The UV-vis absorption spectra were plotted to characterize the colorimetric sensor assembly under optimal conditions (0.5 mL 100 μM H_2O_2, 3.5 mL TMB, 1 mL Fe–Ni@$Ti_3C_2T_x$, 50 °C, 13 min, pH = 3). As shown in Fig. S9, the absorption spectrum of H_2O_2 tends to 0, and no characteristic absorption peak was observed. After the addition of TMB, a smaller absorption peak appeared at 650 nm. This was attributed to the strong oxidizing properties of H_2O_2, which can decompose a small amount of –OH to oxidize TMB even without catalysis by peroxidase. Finally, by adding Fe–Ni@$Ti_3C_2T_x$, the absorption peak at 650 nm increased significantly due to the excellent dual enzyme activities of Fe–Ni@$Ti_3C_2T_x$, which can consume O_2 to produce H_2O_2 and catalyze the production of large amounts of –OH from H_2O_2 to oxidize TMB. The above conclusions indicated that the prepared colorimetric sensor achieved the expected results. The impact of H_2O_2 concentration on the absorbance at 650 nm under the optimal experimental conditions is presented in Fig. 4A. In the range of 50–6000 μM, the absorbance gradually increased with the increase in H_2O_2 concentration. The absorbance of the H_2O_2 + TMB + Fe–Ni@$Ti_3C_2T_x$ system showed a good linear relationship with the concentration of H_2O_2, with the linear equation $y = 0.000118582x + 3.84262$ and detection limit 14.606 μM ($3\sigma/k$) (Fig. 4B). Table. S1 compares the results of various reports for the detection of H_2O_2.[34–40]

The detection materials and their ratios employed in different experiments can influence the enzyme-like activity of MXene-based materials. The structural and compositional diversity of MXene materials ($Ti_3C_2T_x$, Nb_2CT_x, and Mo_2CT_x) confers superior catalytic performance when hybridized with heterogeneous components, thereby expanding their applicability across biomedicine,[41] electronic engineering,[42] environmental remediation,[43] and renewable energy sectors.[44] Specifically, the CdS/Ti_3C_2 heterojunction system facilitates multi-electron reduction pathways, enabling efficient H_2 evolution catalysis.[45] Nitrogen-doped Ti_3C_2 quantum dots

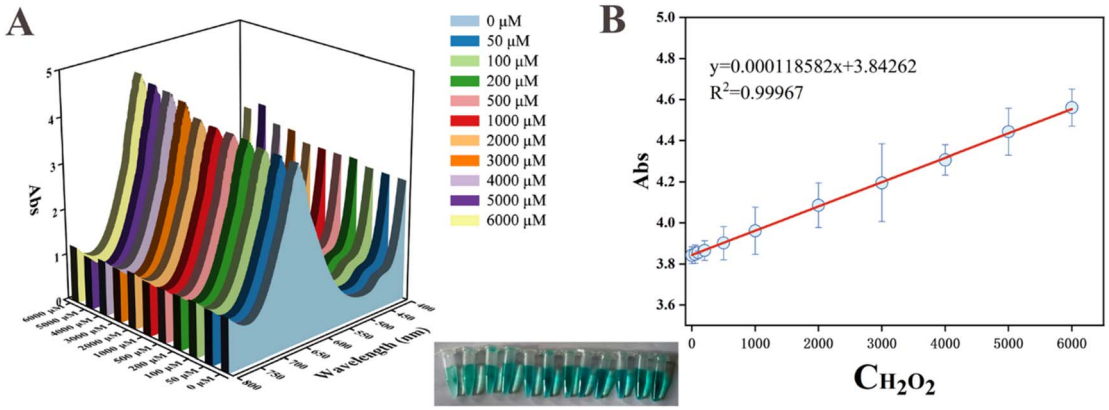

Fig. 4 (A) UV–vis absorption spectra of the colorimetric sensor with different concentrations of H_2O_2 (50–6000 μM). (B) Linear calibration plot of H_2O_2 detection.

enable sensitive H_2O_2 detection through catalytic photoinduced electron transfer mechanisms.[46] MXene-supported metal phosphide composites (NiCoP@$Ti_3C_2T_x$) exhibit dual-functional catalytic behavior: under alkaline conditions, they mediate OH^- adsorption and subsequent H_2O formation, while under acidic environments, they promote H^+ reduction—both processes synergistically accelerating the hydrogen evolution reaction.[47] This study selected the most commonly used $Ti_3C_2T_x$, whose physicochemical properties are well established. Its combination with bimetallic components facilitated a more effective investigation of enzyme-mimetic properties, thereby enhancing the credibility of the results. Compared to other studies utilizing MXene-based materials for H_2O_2 detection, the present approach offered several advantages, including a detection mechanism that enables triple synergistic effects, a stable detection system, convenient operation, and low cost. In conclusion, the colorimetric sensor based on Fe–Ni@$Ti_3C_2T_x$ showed a wide linear range and a low detection limit due to its peroxidase-like and oxidase-like activities, which provided a simple method for the detection of H_2O_2.

3.6 Selectivity, stability and reproducibility tests

The specificity of the colorimetric sensor for H_2O_2 was assessed by comparing the absorbance of the sensor in the presence or absence of interfering substances. K^+, Na^+, Al^{3+}, Cr^{3+}, Li^+, Ca^{2+}, Mn^{2+}, F^-, HPO_4^{2-}, CO_3^{2-}, and NO_3^- were selected as potential interfering substances, with concentrations nearly 100-fold higher than that of H_2O_2. As presented in Fig. 5A, except for CO_3^{2-} and NO_3^-, other interferences had no significant effect on the detection of H_2O_2, which may be attributed to the strong oxidation of H_2O_2, and both CO_3^{2-} and NO_3^- undergo redox reactions with H_2O_2. In other words, they would not coexist in a real environment. Therefore, the specificity of the colorimetric sensor is acceptable.

In practice, the stability of the catalyst is an important factor that affects the whole reaction system. The stability of this colorimetric sensor was examined by storing Fe–Ni@$Ti_3C_2T_x$ at 4 °C for 0, 1, 2 and 3 weeks. As revealed in Fig. 5B, the peroxidase activity of Fe–Ni@$Ti_3C_2T_x$ to various concentrations of H_2O_2 (100 μM, 1000 μM, and 3000 μM) remained basically unchanged, indicating that the colorimetric sensor based on Fe–Ni@$Ti_3C_2T_x$ for the detection of H_2O_2 showed good stability.

In order to evaluate the reproducibility of this colorimetric sensor, the same nine sets of systems were prepared for simultaneous detection with 100 μM, 1000 μM, and 3000 μM H_2O_2. As presented in Fig. 5C, the relative standard deviation (RSD) for 100 μM, 1000 μM, and 3000 μM H_2O_2 was 5.64%, 2.67%, and 2.95%, respectively, suggesting that this colorimetric sensor had a good reproducibility.

3.7 Detection of real samples

In order to evaluate the applicability of this colorimetric sensor for the detection of H_2O_2 in real samples, the recovery of H_2O_2 was analyzed using both blank spiked recovery and sample

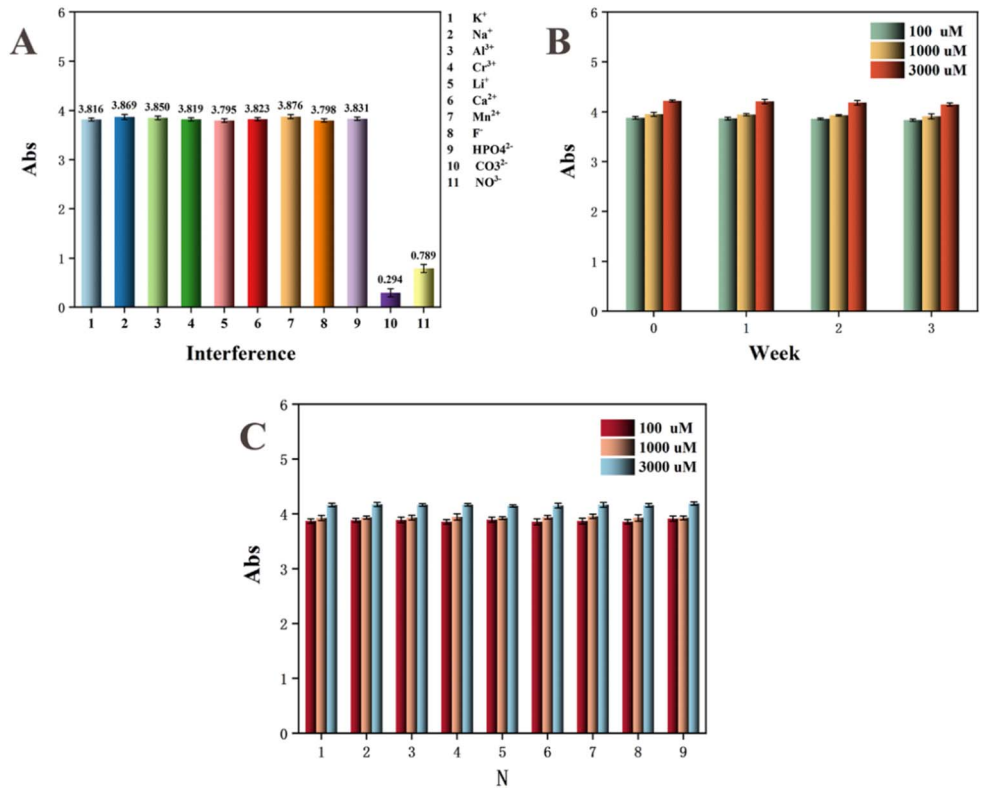

Fig. 5 (A) Absorbance of the reaction system toward interfering species. (B) Absorbance of the reaction system after 0, 1, 2, and 3 weeks. (C) Absorbance of the reaction system under the same conditions in 9 groups.

Table 1 Determination of H_2O_2 in milk using the as-prepared colorimetric sensor

Type	Add (μM)	Sample 1	Sample 2	Sample 3	Found (μM)	Recovery (%)	RSD (%)
Blank	500	543	536	516	531.87	106.37%	2.63%
	1000	952	974	965	963.90	96.39%	1.15%
	3000	2977	3044	3075	3032.41	101.08%	1.65%
Milk	500	547	522	495	521.53	104.31%	4.99%
	1000	986	1014	1077	1025.91	102.59%	4.54%
	3000	3036	3125	2921	3027.75	100.92%	3.38%

spiked recovery. The recoveries for 500 μM, 1000 μM, and 3000 μM H_2O_2 were 106.37%, 96.39%, and 101.08%, with RSDs of 2.63%, 1.15%, and 1.65%, respectively (Table 1). After centrifuging the milk purchased from a local supermarket for 2 h, 500 μM, 1000 μM, and 3000 μM of H_2O_2 were added, and the recoveries were 104.31%, 102.59% and 100.92%, with RSDs of 4.99%, 4.54% and 3.38%, respectively, which indicated that the colorimetric sensor was suitable for the detection of H_2O_2 in real samples.

4 Conclusion

In summary, a novel bimetallic artificial nano-enzyme Fe–Ni@$Ti_3C_2T_x$ with peroxidase-like or oxidase-like activities based on $Ti_3C_2T_x$ was prepared *via* a simple method. Fe–Ni@$Ti_3C_2T_x$ can catalyze the production of –OH from H_2O_2 by multiple mechanisms, and then oxidize the colorless TMB to the colored oxTMB. A sensitive, efficient, convenient and economical colorimetric sensor based on Fe–Ni@$Ti_3C_2T_x$ was constructed for the detection of H_2O_2 to validate the dual enzyme activities and practical applicability of Fe–Ni@$Ti_3C_2T_x$, laying the groundwork for the application of bimetallic nano-enzymes with multiple enzymatic activities.

Author contributions

Zhiren Zhou: data curation, formal analysis, investigation, software, visualization, writing-original draft. Lina Zou: formal analysis, investigation, methodology, project administration, software, writing-original draft. Ping Zhang: data curation, formal analysis, investigation. Jing Dong: data curation, formal analysis, investigation. Jian Zhou: data curation, formal analysis, investigation. Hao Jiang: data curation, formal analysis, investigation. Huanyu Ren: data curation, formal analysis, investigation. Zheng Li: data curation. Huiru Niu: data curation. Hao Liao: data curation. Xiaojing Zhang: data curation. Shanshan An: data curation. Fei Ren: data curation. Xiuhong Ge: data curation. Lang Cheng: data curation. Feiyan Yang: data curation. Hongzhi Pan: methodology. Shengzhong Rong: methodology, project administration, supervision, validation, writing-review & editing. Hongkun Ma: methodology, project administration.

Conflicts of interest

The authors declare no conflict of interest.

Data availability

The data that support the findings of this study are available from the corresponding author on request.

Supplementary information (SI) is available. See DOI: https://doi.org/10.1039/d5na00939a.

Acknowledgements

This research was financially supported by the Fundamental Research Funds for the Universities of Heilongjiang Province (2024-KYYWF-0455).

References

1 M. A. Komkova, E. E. Karyakina and A. A. Karyakin, *J. Am. Chem. Soc.*, 2018, **140**, 11302–11307.
2 Y. Song, K. Qu, C. Zhao, J. Ren and X. Qu, *Adv. Mater.*, 2010, **22**, 2206–2210.
3 Y. Gao, K. Wu, H. Li, W. Chen, M. Fu, K. Yue, X. Zhu and Q. Liu, *Sens. Actuators, B*, 2018, **273**, 1635–1639.
4 H. Geng, Z. Li, Q. Liu, Q. Yang, H. Jia, Q. Chen, A. Zhou and W. He, *Dalton Trans.*, 2022, **51**, 11693–11702.
5 K. Fan, C. Cao, Y. Pan, D. Lu, D. Yang, J. Feng, L. Song, M. Liang and X. Yan, *Nat. Nanotechnol.*, 2012, **7**, 459–464.
6 Z. Chen, J.-J. Yin, Y.-T. Zhou, Y. Zhang, L. Song, M. Song, S. Hu and N. Gu, *ACS Nano*, 2012, **6**, 4001–4012.
7 M. Lejars, A. Margaillan and C. Bressy, *Chem. Rev.*, 2012, **112**, 4347–4390.
8 X. Zhu, P. Song, S. Hou, H. Zhao, Y. Gao, T. Wu and Q. Liu, *Appl. Clay Sci.*, 2023, **242**, 107022.
9 H. Wei, L. Gao, K. Fan, J. Liu, J. He, X. Qu, S. Dong, E. Wang and X. Yan, *Nano Today*, 2021, **40**, 101269.
10 X. Xi, X. Peng, C. Xiong, D. Shi, J. Zhu, W. Wen, X. Zhang and S. Wang, *Microchim. Acta*, 2020, **187**, 1–11.
11 C. Gu, X. Kong, S. Yan, P. Gai and F. Li, *ACS Sustain. Chem. Eng.*, 2020, **8**, 16549–16554.
12 L. Yu, J. Chang, X. Zhuang, H. Li, T. Hou and F. Li, *Anal. Chem.*, 2022, **94**, 3669–3676.
13 M. Naguib, M. Kurtoglu, V. Presser, J. Lu, J. Niu, M. Heon, L. Hultman, Y. Gogotsi and M. W. Barsoum, *Adv. Mater.*, 2011, **23**, 4248–4253.
14 M. Naguib, V. N. Mochalin, M. W. Barsoum and Y. Gogotsi, *Adv. Mater.*, 2014, **26**, 992–1005.
15 S. M. George and B. Kandasubramanian, *Ceram. Int.*, 2020, **46**, 8522–8535.

16 N. Kurra, B. Ahmed, Y. Gogotsi and H. N. Alshareef, *Adv. Energy Mater.*, 2016, **6**, 1601372.
17 J. Ran, G. Gao, F.-T. Li, T.-Y. Ma, A. Du and S.-Z. Qiao, *Nat. Commun.*, 2017, **8**, 13907.
18 J. Zheng, J. Diao, Y. Jin, A. Ding, B. Wang, L. Wu, B. Weng and J. Chen, *J. Electrochem. Soc.*, 2018, **165**, B227.
19 T. Ai, X. Feng and W. Li, *Aerosp. Mater. Technol.*, 2009, **39**, 7–11.
20 M. Lu, W. Han, H. Li, W. Zhang and B. Zhang, *J. Energy Chem.*, 2020, **48**, 344–363.
21 S. Siva, G. A. Bodkhe, C. Cong, S. H. Kim and M. Kim, *J. Ind. Eng. Chem.*, 2023, **124**, 523–531.
22 H. Li, Y. Wen, X. Zhu, J. Wang, L. Zhang and B. Sun, *ACS Sustain. Chem. Eng.*, 2019, **8**, 520–526.
23 H. Zhang, W. Cheng, D. Luan and X. W. Lou, *Angew. Chem., Int. Ed.*, 2021, **60**, 13177–13196.
24 H. Xi, H. Gu, Y. Han, T. You, P. Wu, Q. Liu, L. Zheng, S. Liu, Q. Fu and W. Chen, *Nano Res.*, 2023, 1–8.
25 C. B. Ma, Y. Xu, L. Wu, Q. Wang, J. J. Zheng, G. Ren, X. Wang, X. Gao, M. Zhou and M. Wang, *Angew. Chem., Int. Ed.*, 2022, **61**, 202116170.
26 V. M. Chernyshev and V. P. Ananikov, *ACS Catal.*, 2022, **12**, 1180–1200.
27 M. Sun, K. Pu, X. Hao, T. Liu, Z. Lu, G. Su, C. Wu, Y. Wang, S. Cai and X. Zhao, *J. Mater. Chem. C*, 2024, **12**, 221–231.
28 C. F. Li, L. J. Xie, J. W. Zhao, L. F. Gu, H. B. Tang, L. Zheng and G. R. Li, *Angew Chem. Int. Ed. Engl.*, 2022, **61**, e202116934.
29 J. Hu, Z. Jia, S. Zhao, W. Wang, Q. Zhang, R. Liu and Z. Huang, *Bioresour. Technol.*, 2021, **340**, 125600.
30 M. C. Biesinger, B. P. Payne, A. P. Grosvenor, L. W. Lau, A. R. Gerson and R. S. C. Smart, *Appl. Surf. Sci.*, 2011, **257**, 2717–2730.
31 F. Qi, M. Wu, S. Liu, W. Mu, C. Wu, X. Ren, C. Rui, F. Wu, D. Chang and H. Pan, *Talanta*, 2024, 125606.
32 H. Wang and Z. Ma, *Biosens. Bioelectron.*, 2020, **169**, 112644.
33 Y. Lu, W. Ye, Q. Yang, J. Yu, Q. Wang, P. Zhou, C. Wang, D. Xue and S. Zhao, *Sens. Actuators, B*, 2016, **230**, 721–730.
34 L. Zhao, J. Song, Y. Xue, X. Zhao, Y. Deng, Q. Li and Y. Xia, *Catal. Lett.*, 2018, **148**, 3248–3256.
35 Q. Liu, Y. Jiang, L. Zhang, X. Zhou, X. Lv, Y. Ding, L. Sun, P. Chen and H. Yin, *Mater. Sci. Eng. C*, 2016, **65**, 109–115.
36 T. Wu, F. Liu, X. Lyu, F. Wu, H. Zhao, Y. Xin, L. Li, G. Fan, X. Zhu and Q. Liu, *New J. Chem.*, 2023, **47**, 7575–7582.
37 X. Wen, M. Long and A. Tang, *J. Electroanal. Chem.*, 2017, **785**, 33–39.
38 X. Cao, H. Yang, Q. Wei, Y. Yang, M. Liu, Q. Liu and X. Zhang, *Inorg. Chem. Commun.*, 2021, **123**, 108331.
39 A. Mohan Arjun, N. Shabana, M. Ankitha and P. Abdul Rasheed, *Microchem. J.*, 2023, **185**, 108301.
40 B. Fariba and B. Hadi, *Surf. Eng. Appl. Electrochem.*, 2021, **57**, 708–714.
41 Y. Cheng, B. Jiang, S. Chaemchuen, F. Verpoort and Z. Kou, *Carbon Neutralization*, 2023, **2**, 213–234.
42 L. Li and Q. Cheng, *Exploration*, 2022, **2**, 20220049.
43 M. A. Nazir, T. Najam, S. Ullah, I. Hossain, M. S. Javed, M. Naseer, A. u. Rehman and S. S. A. Shah, *EcoEnergy*, 2024, **2**, 505–548.
44 H. Su, C. Jin, X. Zhang, Z. Yu and X. Zeng, *Carbon Neutralization*, 2024, **3**, 1009–1035.
45 J.-Y. Li, Y.-H. Li, F. Zhang, Z.-R. Tang and Y.-J. Xu, *Appl. Catal., B*, 2020, **269**, 118783.
46 Q. Lu, J. Wang, B. Li, C. Weng, X. Li, W. Yang, X. Yan, J. Hong, W. Zhu and X. Zhou, *Anal. Chem.*, 2020, **92**, 7770–7777.
47 H.-J. Niu, Y. Yan, S. Jiang, T. Liu, T. Sun, W. Zhou, L. Guo and J. Li, *ACS Nano*, 2022, **16**, 11049–11058.